

**Robust nonergodicity of the ground states in the  $\beta$  ensemble**Adway Kumar Das <sup>1,\*</sup>, Anandamohan Ghosh <sup>1,†</sup> and Ivan M. Khaymovich <sup>2,3,‡</sup><sup>1</sup>*Indian Institute of Science Education and Research Kolkata, Mohanpur 741246, India*<sup>2</sup>*Nordita, Stockholm University and KTH Royal Institute of Technology Hannes Alfvéns väg 12, SE-106 91 Stockholm, Sweden*<sup>3</sup>*Institute for Physics of Microstructures, Russian Academy of Sciences, 603950 Nizhny Novgorod, GSP-105, Russia*

(Received 28 November 2023; revised 30 January 2024; accepted 31 January 2024; published 22 February 2024)

In various chaotic quantum many-body systems, the ground states show nontrivial athermal behavior despite the bulk states exhibiting thermalization. Such athermal states play a crucial role in quantum information theory and its applications. Moreover, any generic quantum many-body system in the Krylov basis is represented by a tridiagonal Lanczos Hamiltonian, which is analogous to the matrices from the  $\beta$  ensemble, a well-studied random-matrix model with level repulsion tunable via the parameter  $\beta$ . Motivated by this, here we focus on the localization properties of the ground and anti-ground states of the  $\beta$  ensemble. Both analytically and numerically we show that both the edge states demonstrate nonergodic (fractal) properties for  $\beta \sim \mathcal{O}(1)$ , while the typical bulk states are ergodic. Surprisingly, the fractal dimension of the edge states remains three times smaller than that of the bulk states irrespective of the global phase of the  $\beta$  ensemble. In addition to the fractal dimensions, we also consider the distribution of the localization centers of the spectral edge states, their mutual separation, as well as the spatial and correlation properties of the first excited states.

DOI: [10.1103/PhysRevB.109.064206](https://doi.org/10.1103/PhysRevB.109.064206)**I. INTRODUCTION**

The physics of thermalization in isolated quantum many-body systems has intrigued the condensed matter community over the last few decades [1–4]. The quantum analog of the classical Boltzmann ergodicity hypothesis, named the eigenstate thermalization hypothesis (ETH), claims that in general, an isolated quantum chaotic system will locally thermalize under its own unitary evolution where any local information on the initial state will be lost. Such generic systems play a crucial role in quantum information theory due to their nonequilibrium dynamics [5].

Typically ETH is probed for the highly excited bulk states lying at the center of the energy spectrum where the density of states has the largest value. However, the ground states are particularly important, as they play a major role in the conventional (low-energy) physics of complex and correlated systems while driving collective phenomena like superconductivity [6], fractional quantum Hall effect [7], and others. Compared to the bulk states, the ground states are also more accessible analytically, e.g., through renormalization group methods [8], numerically using tensor-network and quantum Monte Carlo methods [9], and experimentally in quantum simulators using variational algorithms [10,11] in the current noisy intermediate-scale quantum era. In this sense some counterintuitive properties of the ground states of generic many-body systems have drawn a lot of attention since a series of seminal works was published [12–14].

Indeed, in the case of paradigmatic models like Ising and Heisenberg spin- $\frac{1}{2}$  chains [8,13,15] and the Bose-Hubbard model [16], the ground states do not show ergodic behavior, despite the mid-spectrum states exhibiting thermalization. Instead, the ground states demonstrate ergodicity breaking, both in terms of the equipartition over degrees of freedom (i.e., being fractal states that occupy only measure zero of all the Hilbert-space configurations) and entanglement [17]. The ground-state entanglement leads to long-range correlations at zero temperature, producing quantum phase transition, e.g., in the Ising [18,19] and Lipkin-Meshkov-Glick model [20], and Mott insulator-superfluid transitions in bosonic systems [21]. In addition, the empirical probability distribution of ground states for various disordered many-body systems has been recently addressed in several papers; see, e.g., Ref. [22].

The many-body systems are notoriously difficult to handle for larger system sizes due to exponentially increasing Hilbert space dimensions. Following a recent analogy between a tridiagonal Lanczos Hamiltonian in the basis of Krylov operators for a generic quantum many-body system and the  $\beta$  ensemble [23,24], we consider the ground-state properties of the latter, being the proxy of the above many-body interacting systems. In the case of the  $\beta$  ensemble, the ground-state energy can be related to the stochastic Airy operators [25], while its density can be expressed in terms of the multivariate integrals [26]. The relevant Tracy-Widom laws for arbitrary  $\beta$  have been extensively studied [27–31]. In particular, for  $\beta \rightarrow 0$  the Tracy-Widom distributions weakly converge to the Gumbel distribution in the thermodynamic limit [32,33]. Recently a recursion relation was proposed for the probability distribution of the ground-state energy of the Laguerre  $\beta$  ensemble [34].

\*akd19rs062@iiserkol.ac.in

†anandamohan@iiserkol.ac.in

‡ivan.khaymovich@gmail.com

In this work we look at the structure of the ground state of the Gaussian  $\beta$  ensemble. We find that in the nonergodic extended phase the fractal dimension of the ground state is  $1/3$  of the typical bulk fractal dimension. In the weak disorder limit of the one-dimensional (1D) Anderson model [35], the localization length of the ground state also scales with an exponent  $1/3$  compared to the highly excited bulk states. We will show that our result for the  $\beta$  ensemble can be explained from an equivalence to the 1D Anderson model. Similar to the many-body quantum chaotic systems, the ground states of the  $\beta$  ensemble exhibit nonergodic structure for  $\beta \sim \mathcal{O}(1)$ , when the typical bulk states are known to be ergodic [36]. We also show that the fractal dimension of the ground state is  $1/3$  of the bulk states even in the extended phase,  $\beta \gtrsim 1$ . This feature will be explained from a correspondence to the mean Hamiltonian model [37,38].

The rest of the paper is organized as follows. Section II describes the model in focus, summarizing the main properties of the  $\beta$  ensemble. In Sec. III we consider both numerically and analytically the ground-state properties of the nonergodic phase of the model, focusing on the fractal dimensions of the ground state and the statistics of the localization centers. In Sec. IV we look at the ground state in the extended phase ( $\beta \gtrsim 1$ ), shown to be dominated by a deterministic part of the Hamiltonian. Section V summarizes our results.

## II. MODEL

### A. Model description

The  $\beta$  ensemble is a random-matrix model with a joint probability distribution of eigenvalues known exactly and controlled only by the Dyson's index  $\beta$ , interpreted as the inverse temperature of an equivalent Coulomb gas model [39,40]. Consequently, the standard joint probability distributions of the Gaussian ensembles, with  $\beta = 1, 2$ , and  $4$ , depending on the symmetry, are generalized over any real  $\beta$  values in case of the  $\beta$  ensemble. Such an ensemble consists of real symmetric tridiagonal matrices having independent random elements [41]. The corresponding symmetric  $N \times N$  Hamiltonian matrix  $H$  has the following nonzero elements,  $H_{m,n}$ ,  $1 \leq m \leq n \leq N$ :

$$H_{n,n} \sim \mathcal{N}(0, 1), \quad H_{n,n+1} = y_n, \quad \sqrt{2}y_n \sim \chi_{n\beta}, \quad (1)$$

where the diagonal elements obey the Gaussian distribution  $\mathcal{N}(0, 1)$ , with zero mean and unit variance, while the off-diagonal ones follow the Chi distribution  $\chi_{n\beta}$ , with the site index  $n$ -dependent width parameter  $n\beta$ ,  $1 \leq n \leq N$ . In the above site basis,  $H$  represents a random single-particle model on a 1D lattice with open boundary conditions and site-dependent hopping term [38]. The relative strength of the on-site ( $H_{n,n}$ ) and the hopping terms ( $y_n$ ) at a typical site  $n \sim \mathcal{O}(N)$  indicate a suitable scaling of the system parameter  $\beta = N^{-\gamma}$ , where  $\gamma$  is a certain real-valued parameter [36,42,43].

### B. Bulk phase diagram

Equation (1) implies that the hopping amplitudes increase on average along the lattice as  $\langle y_n \rangle = \sqrt{\beta n}$  for  $\beta n \gtrsim 1$  and present a highly inhomogeneous system. Such inhomogeneity

allows for phase transitions in the  $\beta$  ensemble, whereas criticality is forbidden in a generic 1D system with uncorrelated short-range hopping [44,45]. Particularly, for all the typical bulk states, there are the Anderson transition at  $\gamma = 1$  and the ergodicity breaking transition at  $\gamma = 0$ , leading to a nonergodic extended (NEE) phase for  $0 < \gamma < 1$ . Therefore, other than long-range hopping [46,47], quasiperiodicity [48], drive [49], interaction [50], or correlated disorder [51], inhomogeneity in short-range hopping strength is another ingredient for phase transition in 1D systems. Apart from the hopping terms, inhomogeneous interaction [52] or inhomogeneity in on-site terms can lead to criticality as well, e.g., Wannier-Stark localization induced by linear potential [53].

In the ergodic regime of the  $\beta$  ensemble, the bulk eigenstates span over the entire Hilbert space and the eigenvalues are correlated over distances much larger than the mean level spacing [54]. The degree of energy correlation is controlled by  $\beta$  [55] such that the standard Wigner-Dyson level repulsion is observed for  $\beta \sim \mathcal{O}(1)$ . Contrarily, the localized phase ( $\gamma > 1$ ) reflects the characteristics of the integrable systems where all the eigenvalues are uncorrelated and the eigenstates are spatially localized [56].

In the NEE phase, the typical bulk eigenstates are fractal with the dimension  $D_2 = 1 - \gamma$ , given by the scaling of the inverse participation ratio (IPR), which is the second moment of the density of the eigenstate intensities,

$$I_2 = \sum_n |\Psi_E(n)|^4 \sim N^{-D_2}, \quad (2)$$

where  $\Psi_E(n)$  is the  $n$ th component of the eigenstate at energy  $E$  in the chosen basis. The fractional value  $0 < D_2 < 1$  implies that the typical bulk states occupy an extensive part but vanishing fraction of the Hilbert space. Such NEE states are observed in various random-matrix ensembles [46,51,57–74], physical models [49,50,75–91], and realized in experimental setups [92–94]. However, in the NEE phase of the  $\beta$  ensemble, nearby eigenvalues remain uncorrelated with nonhybridizing eigenstates but two distant eigenvalues separated by  $\Delta E > N^{\frac{\gamma-1}{2}}$  can be correlated [95]. Moreover, in the middle of the spectrum, a small energy window,  $(-E_G, E_G)$ ,  $E_G \sim \mathcal{O}(1)$ , contains  $\mathcal{O}(N^\gamma)$  localized states along with the NEE states without forming any mobility edge [36], therefore challenging Mott's argument [96]. Such emergence of localized or extended states at a given energy in different realizations of  $\beta$  ensemble for  $0 < \gamma < 1$  can be attributed to three ingredients: residual level repulsion, nonergodicity of most bulk states, and spatial separation of extended and localized states. These criteria have been recently identified and demonstrated in case of the  $\beta$  ensemble [36]. The distinct eigenstate and eigenvalue structure in the NEE phase of  $\beta$  ensemble can be analytically understood from a spatially local mapping to the 1D Anderson model with  $N$ -dependent hopping strength [36]. Such spatially local mapping can also explain the behavior of the ground state of the  $\beta$  ensemble, as we show in this work.

## III. GROUND STATE IN THE NEE PHASE

We start this section with the numerical exploration of the ground  $|\Psi^-\rangle$  and anti-ground  $|\Psi^+\rangle$  eigenstates of (1) at both

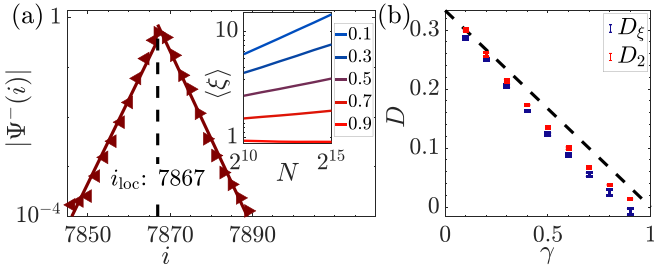


FIG. 1. Ground-state exponential decay. (a) Ground-state components  $\Psi^-(i)$  vs lattice index  $i$  from a single realization of  $\beta$  ensemble for  $N = 8192$ ,  $\gamma = 0.5$  where  $i_{\text{loc}}$  is the localization center, i.e., the location of the wave-function intensity maximum. Markers denote raw data and solid lines denote linear fit of  $\ln |\Psi^-(i)|$  vs  $|i - i_{\text{loc}}|$ , Eq. (3). Inset shows the ensemble-averaged decay length scale  $\xi$  vs the system size  $N$  for various  $\gamma$ . (b) Fractal dimensions of ground state vs  $\gamma$  where the dashed line denotes  $D = \frac{1-\gamma}{3}$ .  $D_2$  and  $D_\xi$  extracted from the system-size scaling of the typical IPR, Eq. (2), and  $\xi$ , i.e.,  $\langle \ln I_2 \rangle \propto -D_2 \ln N$  and  $\langle \ln \xi \rangle \propto D_\xi \ln N$  for  $2^{10} \leq N \leq 2^{15}$ . Error bars denote 95% confidence interval.

the smallest and the largest eigenenergies. In Secs. III A and III B we focus on the scaling properties, the spatial spread, and the localization-center distribution of  $|\Psi^\pm\rangle$  separately. Section III C is devoted to the correlations between  $|\Psi^+\rangle$  and  $|\Psi^-\rangle$ . In Sec. III D we provide analytical explanation of the numerical results.

### A. Ground-state fractal dimension

In Fig. 1(a) we plot the absolute values of the ground-state components with regard to the lattice indices from a single realization of the  $\beta$  ensemble for  $N = 8192$  and  $\gamma = 0.5$ . Even for a single realization, the exponential decay of the ground state  $|\Psi^-\rangle$  is immediately apparent, i.e.,

$$|\Psi^-(i)| \sim \exp\left(-\frac{|i - i_{\text{loc}}|}{\xi}\right), \quad (3)$$

where  $\xi$  is the decay length scale and  $i_{\text{loc}}$  is the localization center, where the eigenstate has the largest intensity. In the inset of Fig. 1(a) we show that the ensemble-averaged decay length scale  $\langle \xi \rangle$  has a power-law scaling with regard to the system size, i.e.,  $\langle \xi \rangle \propto N^{D_\xi}$ . In Fig. 1(b) we show that  $D_\xi \approx \frac{1-\gamma}{3}$  for  $0 \leq \gamma \leq 1$ . We find that the fractal exponent  $D_2$ , defined by the system-size scaling of the IPR for the ground state  $|\Psi^-\rangle$ , Eq. (2), is consistent with  $D_\xi$ , i.e.,  $D_2 \approx \frac{1-\gamma}{3}$ . We further observe the anti-ground state,  $|\Psi^+\rangle$ , i.e., the eigenstate with the largest energy also has the same fractal dimension  $\frac{1-\gamma}{3}$ .

Note that the typical bulk eigenstates have the fractal dimension  $D_{\text{bulk}} \sim 1 - \gamma$ , i.e., three times that of the spectral edge states. Moreover, in the Appendix we compare the distribution of IPR of the bulk and ground states, see Fig. 5. We show that, unlike the distribution of IPR of the bulk states, which is bimodal and fat-tailed, see Fig. 5(a), the corresponding ground-state IPR distribution is well described by a Gaussian distribution with both mean and standard deviation scaling as  $N^{\frac{1-\gamma}{3}}$ , see Fig. 5(b).

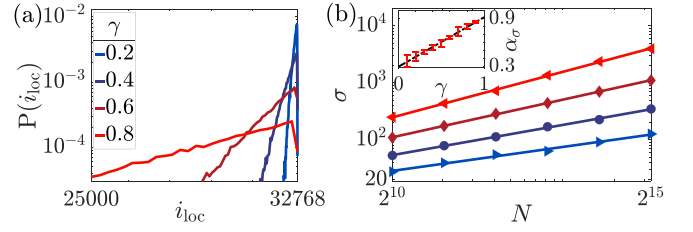


FIG. 2. Ground-state localization-center distribution. (a) Probability distribution  $P(i_{\text{loc}})$  of the localization center  $i_{\text{loc}}$  of the ground states for various  $\gamma$  and  $N = 32768$ . (b) Width of  $P(i_{\text{loc}})$  vs  $N$  for various  $\gamma$ , extracted from an exponential tail,  $P(i_{\text{loc}}) \propto \exp(-\frac{i_{\text{loc}}}{\sigma})$ . The markers and solid lines denote raw data and linear fit in log-log scale, respectively. The inset shows the system-size scaling  $\alpha_\sigma$  of  $\sigma \propto N^{\alpha_\sigma}$  as a function of  $\gamma$ , where the dashed line denotes  $\alpha_\sigma = \frac{2\gamma+1}{3}$ .

### B. Localization center

Next we consider the spatial distribution of the localization centers  $i_{\text{loc}}$  of the ground state. We find that the typical  $i_{\text{loc}}$  scales linearly with  $N$ , Fig. 5(c), i.e., the ground state has the largest probability to stay near the right edge of the lattice. In Fig. 2(a) we show the spatial distribution of  $i_{\text{loc}}$  for  $N = 32768$  and various values of  $\gamma$ . The exponential tails of such distributions imply that  $P(i_{\text{loc}}) \propto \exp(-\frac{i_{\text{loc}}}{\sigma})$ , where  $\sigma$  is the width of the distribution. Figure 2(b) demonstrates that  $\sigma$  increases with  $N$  in a power-law manner while the system-size scaling exponent  $\alpha_\sigma$ , shown in the inset, indicates that  $\sigma \propto N^{\frac{2\gamma+1}{3}}$ . The same scaling behaviors are also observed in case of the anti-ground state due to (i) the statistical homogeneity of the hopping terms  $H_{mn}$ , i.e.,  $P(H_{mn}) = P(-H_{mn})$ , and (ii) the transformation  $E \rightarrow -E$  leading to  $\Psi_E(n) \rightarrow (-1)^n \Psi_{-E}(n)$  in Eq. (1).

### C. Overlap of ground and anti-ground states $|\Psi^\pm\rangle$

It is now pertinent to ask whether the ground and anti-ground states are correlated with each other, i.e., whether they are formed via a single strong level resonance or via an extensive set of many parametrically smaller ones. To start with, in the inset of Fig. 3(a) we show the locations of the ground and the anti-ground states,  $|\Psi^\pm\rangle$ , from a single realization of the  $\beta$  ensemble for  $N = 8192$  and  $\gamma = 0.3$  and  $0.7$ . One can see that  $|\Psi^\pm\rangle$  has a significant degree of overlap close to the ergodic transition point,  $\gamma = 0$ , while near the Anderson transition point,  $\gamma = 1$ , the overlap is almost negligible. To understand such an overlap with respect to various disorder realizations, we look at the random variable  $|i_{\text{loc}}^+ - i_{\text{loc}}^-|$ , which is the distance between the localization centers of the ground and anti-ground states. As shown in Fig. 3(a), the probability distribution of  $|i_{\text{loc}}^+ - i_{\text{loc}}^-|$  decays exponentially and has a width  $\sigma \propto \frac{3}{2\gamma+1} N^{\frac{2\gamma+1}{3}}$ . The distribution of the rescaled gap,  $\tilde{\Delta} \equiv \frac{|i_{\text{loc}}^+ - i_{\text{loc}}^-|}{\sigma}$ , shown in Fig. 3(a), collapses onto a single curve for different system sizes and parameter values. The same scaling of the widths,  $\sigma$ , of the distributions  $P(i_{\text{loc}}^\pm)$  and  $P(|i_{\text{loc}}^+ - i_{\text{loc}}^-|)$  indicates that the localization centers of the ground and anti-ground states are independent of each other and identically distributed according to the exponential distribution  $\propto \exp(-\frac{2\gamma+1}{3} \frac{i_{\text{loc}}^\pm}{N})$ .

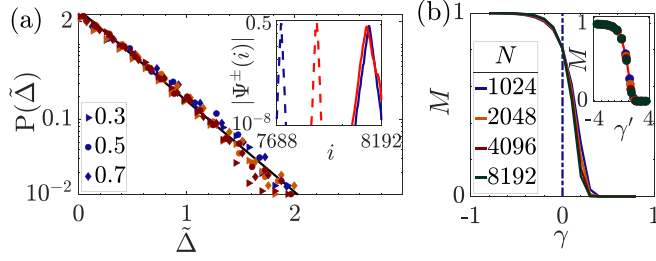


FIG. 3. Correlations of ground and anti-ground states. (a) Probability distribution of the gap  $\hat{\Delta} = |i_{\text{loc}}^+ - i_{\text{loc}}^-|/\sigma$  of localization centers of the ground and anti-ground states, rescaled by  $\sigma = \frac{3}{2\gamma+1}N^{2\gamma+1}$ . Different colors denote three different system sizes,  $N = 1024, 4096, 16384$ . Inset shows the ground (blue) and anti-ground (red) states from a single realization of  $\beta$  ensemble for  $N = 8192$  where  $\gamma = 0.3$  (solid) and  $0.7$  (dashed). (b) Covariance of ground and anti-ground state vs  $\gamma$  for various  $N$ . Inset shows collapsed data where  $\gamma' = \gamma(\log N)^{1/3}$ , with  $\gamma = 0$  being the critical point with the critical exponent  $\nu \approx 1$  [42].

To quantify the overlap of  $|\Psi^\pm\rangle$  more accurately, we compute the covariance,  $M = \sum_i |\Psi^-(i)\Psi^+(i)|$  [36]. For two states with the complete overlap,  $M = 1$ , whereas  $M \rightarrow 0$  for states with no significant hybridization. Figure 3(b) shows that the covariance vs  $\gamma$  for various system sizes shows a crossover from  $M = 1$  deep in the regime  $\gamma < 0$  to  $M \rightarrow 0$  in the NEE phase ( $0 < \gamma < 1$ ). Moreover, the crossover curves tend to intersect at  $\gamma = 0$  and get steeper upon increasing  $N$ . The finite-size collapse of the data, shown in the inset of Fig. 3(b), suggests a second-order phase transition with a critical point at  $\gamma = 0$ . For all values of  $\gamma > 0$ , ground and anti-ground states do not hybridize in the thermodynamic limit, thus confirming the multiple-resonance nature of these states.

#### D. Analytical consideration

We now present an analytical understanding of the above numerical results. Let us begin by recalling that the 1D Anderson model with constant hopping strength  $t$  and disordered on-site potentials  $\epsilon_n$  can be represented as a two-dimensional (2D) classical Hamiltonian map [35,97]:

$$\hat{H} = \sum_{n=1}^N \epsilon_n c_n^\dagger c_n + t \sum_{k=1}^{N-1} c_k c_{k+1}^\dagger + c_k^\dagger c_{k+1} \quad (4)$$

$$\Leftrightarrow \begin{cases} x_{n+1} = x_n \cos \mu - (p_n + A_n x_n) \sin \mu \\ p_{n+1} = x_n \sin \mu + (p_n + A_n x_n) \cos \mu, \end{cases}$$

where  $c_k^\dagger, c_k$  are the creation and annihilation operators at the  $k$ th site and  $(x_n, p_n)$  are the position and momentum of a linear kicked oscillator. In terms of the parameter  $\mu$ , we can express the energy,  $E = 2t \cos \mu$ , and the kick strength,  $A_n = -\frac{\epsilon_n}{t \sin \mu}$ . In [35], it has been shown that in the weak disorder limit,  $|A_n| \ll 1$ , the localization length of the ground/anti-ground state is given by

$$\xi \propto \left( \frac{t^2}{\langle \epsilon_n^2 \rangle} \right)^{1/3}. \quad (5)$$

On the other hand, it has been recently shown that for the  $\beta$  ensemble in the NEE phase, there exists a spatially local mapping to the 1D Anderson model with  $N$ -dependent hopping strengths [36]. Specifically, a 1D lattice of length  $N$  governed by the  $\beta$  ensemble can be partitioned into nearly independent spatial blocks  $\Delta_0, \Delta_1, \dots, \Delta_{l_{\text{max}}}$  where the zeroth block represents first  $N^\gamma$  sites,  $\Delta_0 = [1, N^\gamma]$ , and the  $l$ th block for  $l \geq 1$  has the length  $|\Delta_l| \sim N^{\gamma+\zeta_l}$  and is defined as

$$\Delta_l \equiv [N^{\gamma+\zeta_l}, cN^{\gamma+\zeta_l}], \quad \zeta_l = (l-1) \frac{\ln c}{\ln N}, \quad (6)$$

where  $l_{\text{max}} = (1-\gamma) \frac{\ln N}{\ln c}$  and  $c \sim \mathcal{O}(1)$  is a constant. On one hand, within  $\Delta_0$ , the hopping terms are negligible compared to the typical on-site potential  $\mathcal{O}(1)$ ; hence all the sites within are effectively disconnected from the rest of the lattice and host single-site-localized eigenstates. On the other hand, the model in  $\Delta_l$  for  $l \geq 1$  can be shown to be asymptotically equivalent to the 1D Anderson model of length  $|\Delta_l| \sim N^{\gamma+\zeta_l}$  with uncorrelated diagonal disorder  $\mathcal{O}(1)$  and nearly homogeneous hopping  $t \simeq y_{\Delta_l} \sim N^{\zeta_l/2}$  growing with  $l$ . This mapping works in the nonergodic phases at  $\beta \lesssim 1$ .

According to the above mapping, eigenstates are exponentially decaying at a length scale  $\xi_l \sim N^{\zeta_l}$ , and hence the block  $\Delta_l$  consists of  $N^\gamma$  sub-blocks of length  $N^{\zeta_l}$ . In addition, each of these sub-blocks has Gaussian density of states (DOS) with bandwidth  $N^{\zeta_l/2}$  and, thus, the mean level spacing  $\delta_l \sim N^{-\zeta_l/2}$ .

As a result, the last spatial block,  $\Delta_{l_{\text{max}}}$  ( $\zeta_{l_{\text{max}}} = 1 - \gamma$ ), is the largest one containing a finite fraction  $\mathcal{O}(N)$  of states that exponentially decays within the length scale  $N^{1-\gamma}$  and has the largest energy bandwidth  $N^{\frac{1-\gamma}{2}}$  among all possible spatial blocks. Consequently, the ground state of the  $\Delta_{l_{\text{max}}}$  block should coincide with the ground state of the entire  $\beta$  ensemble.

In the  $\Delta_{l_{\text{max}}}$  block,  $t^2 \sim N^{1-\gamma} \gg 1$  and  $\langle \epsilon_n^2 \rangle = 1$  correspond to the weak disorder limit of  $|A_n| \ll 1$  in [35]; hence the decay length scale of the edge states should scale as in Eq. (5), i.e.,  $\xi \sim N^{\frac{1-\gamma}{3}}$ . This explains the fractal dimension of the ground (and anti-ground) state of  $\Delta_{l_{\text{max}}}$  and, thus, of the  $\beta$  ensemble to be  $\frac{1-\gamma}{3}$ , in contrast to the typical bulk states having a fractal dimension  $1 - \gamma$ . This supports the numerical results of Fig. 1. Note that even at the ergodic transition,  $\gamma = 0$ , both the ground and anti-ground states remain nonergodic, with the fractal dimension  $D_2 = 1/3$ , while for the typical bulk states,  $D_2$  reaches its ergodic value of 1. This is fully consistent with the results of the entire extended phase  $\gamma < 0$  in the next section and Fig. 4(c), where formally the above mapping is not applicable.

In order to understand the width of the distribution of the ground-state localization centers, one has to consider the inhomogeneity in the hopping terms within  $\Delta_{l_{\text{max}}}$ . As we have explained above, at the edge of the spectrum, the energy  $E \sim \mathcal{O}(N^{\frac{1-\gamma}{2}})$ , being large compared to the on-site potential  $\epsilon_n \sim \mathcal{O}(1)$ , is determined solely by the hopping amplitude  $y_n \sim \sqrt{n}N^{-\gamma}$ . Thus the ground state with localization center at  $i_{\text{loc}} = N - \sigma$  should have the energy  $E \sim \sqrt{(N - \sigma)N^{-\gamma}}$  and

$$\cos \mu = \frac{E}{2t} = \sqrt{1 - \frac{\sigma}{N}} \approx 1 - \frac{\sigma}{2N}. \quad (7)$$

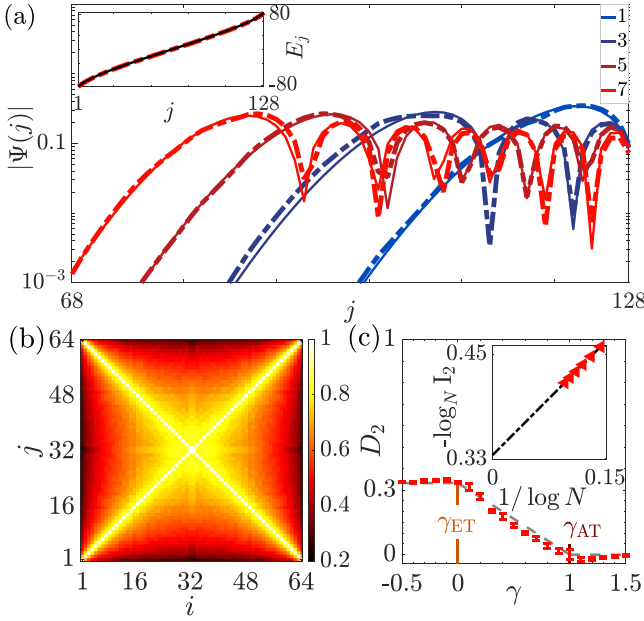


FIG. 4. Eigenstate structure for  $\gamma < 0$ . (a) Ground and first few excited states from a single realization of the  $\beta$  ensemble for  $N = 128$  and  $\gamma = -0.7$  where in the legend, 1 (3) corresponds the ground (second excited) state and so on. Inset shows the eigenspectrum. In both main plot and the inset, dashed (solid) lines correspond to the exact-diagonalization numerical result [analytical expression in Eq. (10)]. (b) Covariance  $M_{ij}$  between all possible pairs of eigenstates  $i$  and  $j$  of  $\bar{H}$  for  $N = 64$ . (c) Fractal dimension  $D_2$  for the ground state of  $\beta$  ensemble vs  $\gamma$ . Error bars denote 95% confidence interval.  $\gamma_{\text{ET}} = 0$  and  $\gamma_{\text{AT}} = 1$  denote the ergodic and Anderson transitions, respectively. Inset shows finite-size fractal dimensions for  $\bar{H}$  as a function of  $1/\log N$ , where extrapolation of  $1/\log N \rightarrow 0$  (i.e.,  $N \rightarrow \infty$ ) estimates  $D_2 = 1/3$ .

For the ground state of  $\Delta_{l_{\text{max}}}$  block,  $\mu \sim t^{-2/3} = N^{-(1-\gamma)/3} \rightarrow 0$  in the weak disorder limit [35]. On the other hand, Eq. (7) implies that for  $\mu \rightarrow 0$ ,

$$\sigma \approx 2N(1 - \cos \mu) \approx N\mu^2 \sim N^{\frac{2\gamma+1}{3}}. \quad (8)$$

Therefore the ground state is likely to have a localization center close to the right edge of the lattice ( $N - i_{\text{loc}} \ll N$ ) and its distribution should have a width scaling as  $\sigma \sim N^{\frac{2\gamma+1}{3}}$ . This confirms the numerical results observed in Figs. 2, 3(a), and 5(c).

All the above results are valid as long as the conditions for (i) the local spatial mapping of [36] and (ii) the weak disorder limit of [35] are satisfied. The latter is applicable in the delocalized phases,  $\gamma < 1$ . Otherwise, all the states, including the ground state, are localized and results can be formally extended to the localized phase. On the other hand, the former local mapping is valid for  $\gamma > 0$ . Thus the uncorrelated nature of the ground and anti-ground states of the 1D Anderson model together with local mapping of [36] confirms the results of Fig. 3(b) that the correlations are absent in all the nonergodic phases,  $\gamma > 0$ . The constraint of local spatial mapping to the 1D Anderson model breaks down as soon as  $\beta \gtrsim 1$ . Hence, the region  $\gamma < 0$  needs to be treated separately, as discussed in the next section.

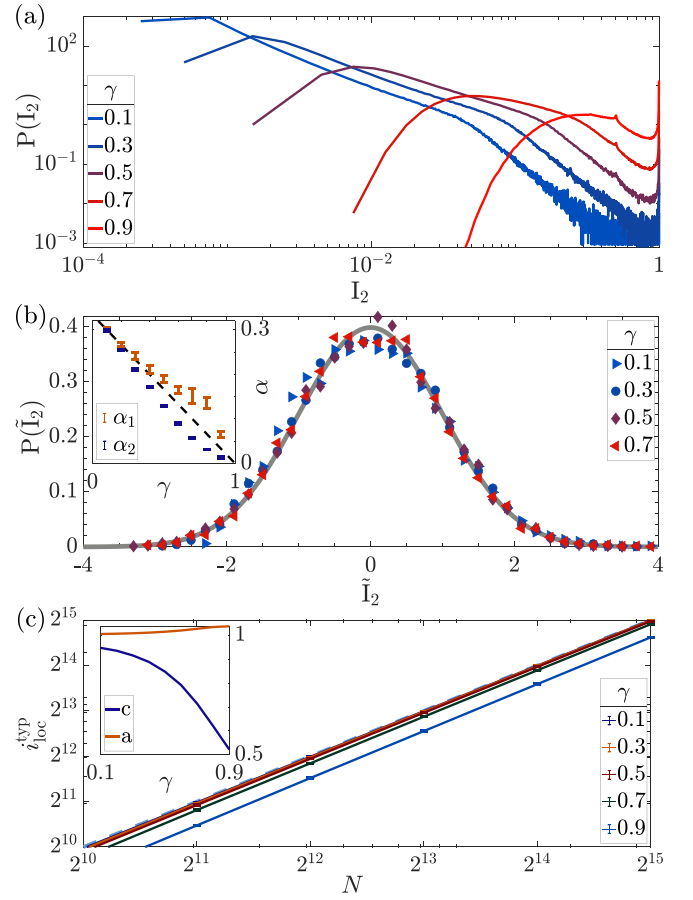


FIG. 5. Comparison of bulk- and ground-state IPR distributions. (a) Probability distribution of IPR of all the eigenstates in log-log scale for various  $\gamma$  and  $N = 8192$ . (b) The collapse of the probability distribution of  $\bar{I}$  of ground state for  $N = 8192$ , where  $\bar{I} = \frac{I-1}{SD(I)}$ , stands for the rescaled fluctuations relative to the standard deviation (SD), while the solid line denotes normal distribution  $\mathcal{N}(0, 1)$ . Inset shows  $SD(I) \propto N^{-\alpha_1}$ ,  $|\Psi^-(i_{\text{loc}})|^2 \propto N^{-\alpha_2}$  where dashed line denotes  $\alpha = D^- \equiv \frac{1-\gamma}{3}$ . (c) Typical ground-state localization center  $i_{\text{loc}}^{\text{typ}}$  vs  $N$ , where dashed line denotes  $i_{\text{loc}}^{\text{typ}} = N$ . Inset shows  $c$  and  $a$  vs  $\gamma$  where  $i_{\text{loc}}^{\text{typ}} = cN^a$ .

#### IV. EXTENDED PHASE FOR $\gamma < 0$

In the region  $\gamma < 0$ , the typical hopping amplitude,  $y_n^{\text{typ}} \sim \frac{\sqrt{nN^{|\gamma|}}}{2}$ , is large for all  $n$  at  $N \gg 1$  and  $y_{n+m} - y_n \sim mN^{\frac{|\gamma|}{2}}/n \gg 1$  even for  $m = 1$ . Thus the smallest mean hopping term is large compared to both the typical on-site terms and off-diagonal fluctuations  $\sim \mathcal{O}(1)$ . Consequently, a Hamiltonian  $H$  from the  $\beta$  ensemble for  $\gamma < 0$  rescaled as  $H \rightarrow \sqrt{2}N^{\frac{\gamma}{2}}H$  can be approximated by its mean [37,38]:

$$\bar{H}_{m,n} = \sqrt{m}\delta_{m,n-1} + \sqrt{m-1}\delta_{m,n+1}. \quad (9)$$

$\bar{H}$  is equivalent to  $\hat{a}^\dagger + \hat{a}$  represented in the first  $N$  eigenstates of the Harmonic oscillator where  $\hat{a}$ ,  $\hat{a}^\dagger$  are the corresponding annihilation and creation operators, respectively. Solving the characteristics equation  $\det(\bar{H} - E\mathbb{1}) = 0$ , we get the eigenstates of  $\bar{H}$  as

$$\Psi_{\lambda_n}(k) = Z_n \frac{\mathcal{H}_{k-1}(\lambda_n)}{\sqrt{2^{k-1}(k-1)!}}, \quad (10)$$

where  $\mathcal{Z}_n$  is a normalization factor and  $\Psi_{\lambda_n}(k)$  is the  $k$ th component of the eigenstate  $|\Psi_{\lambda_n}\rangle$  with energy  $\lambda_n$ , which is the  $n$ th zero of the  $N$ th-order Hermite polynomial,

$$\mathcal{H}_N(x) = (-1)^N e^{x^2} \frac{d^N}{dx^N} e^{-x^2}. \quad (11)$$

The energy of the original Hamiltonian  $H$  from the  $\beta$  ensemble is  $E_n \approx N^{\frac{\nu_1}{2}} \lambda_n$ . For a single realization of the  $\beta$  ensemble with  $N = 128$  and  $\gamma = -0.7$ , we show the ground state and a few excited states in Fig. 4(a) while the eigenvalues are shown in the inset. In the same figure we also show the analytical expressions from Eq. (10) valid for the Hamiltonian  $\bar{H}$ . We observe that the analytical estimates from Eq. (10) perfectly match the results of the exact diagonalization in case of both energy levels and eigenstates, even for a single realization of a  $\beta$  ensemble with a relatively small system size. Thus  $\bar{H}$  is indeed a good approximation of the  $\beta$  ensemble for  $\gamma < 0$ , where exponential decay of the eigenstates observed in the NEE phase is absent.

The largest zero of the Hermite polynomial in Eq. (11) is [98]

$$\lambda^{\max} = \sqrt{2N} + \mathcal{O}(N^{-1/6}). \quad (12)$$

Thus the energy bandwidth of  $\bar{H}$  is  $\sim \sqrt{N}$ . Then we can estimate the bandwidth of the original Hamiltonian  $H$  as  $\sqrt{N} \cdot N^{\frac{\nu_1}{2}} = N^{\frac{1-\gamma}{2}}$  and the mean level spacing as  $\delta \sim N^{-\frac{\gamma+1}{2}}$ . Both of these scalings match with those of the  $\beta$  ensemble for  $\gamma < 0$ .

The eigenstates in Eq. (10) along with the symmetry  $\mathcal{H}_n(-x) = (-1)^n \mathcal{H}_n(x)$  are such that the absolute values of the components of two eigenstates with energy  $\pm E$  are equal. Hence, the  $j$ th and  $(N+1-j)$ th energy-ordered states should fully hybridize with each other and show perfect correlations as shown in Fig. 4(b), inferred from the covariance of each pair of eigenstates. In particular, the ground state  $|\Psi^-\rangle$  and the anti-ground state  $|\Psi^+\rangle$  have perfect overlap in the case of  $\bar{H}$ . As  $\bar{H}$  is a good approximation of the  $\beta$  ensemble for  $\gamma < 0$ ,  $|\Psi^\pm\rangle$  of the  $\beta$  ensemble should have high degree of overlap, which is reflected by  $M$  being close to unity in Fig. 3(b) for  $\gamma < 0$ , where  $M$  is the covariance of  $|\Psi^\pm\rangle$  quantifying their hybridization.

Additionally, we look at the short-range energy correlation at the edge of the spectrum using the level-spacing ratio,  $r$  statistics [99,100]. In the Gaussian orthogonal ensemble, ensemble-averaged  $r$  statistics have a value  $\approx 0.53$ , which is typical for the bulk spectrum of the chaotic quantum systems. On the other hand,  $\langle r \rangle \approx 0.39$  for the Poisson ensemble representing the regular spectrum. In Appendix B we show that at the spectral edges,  $\langle r \rangle \simeq 0.8187$  for  $\bar{H}$ . Such a value of  $r$  statistics is obtained in case of the  $\beta$  ensemble for  $\gamma < 0$  upon increasing system size or decreasing  $\gamma$ , as shown in Fig. 6(a). In contrast,  $\langle r \rangle \rightarrow 1$  in the bulk spectrum, as we get a rigid picket-fence spectrum for  $\gamma < 0$  and  $N \gg 1$ .

### Ground state for $\gamma < 0$

Finally, to explain the behavior of low-energy eigenstates as in Fig. 4(a), we need to look at the expansion of the Hermite

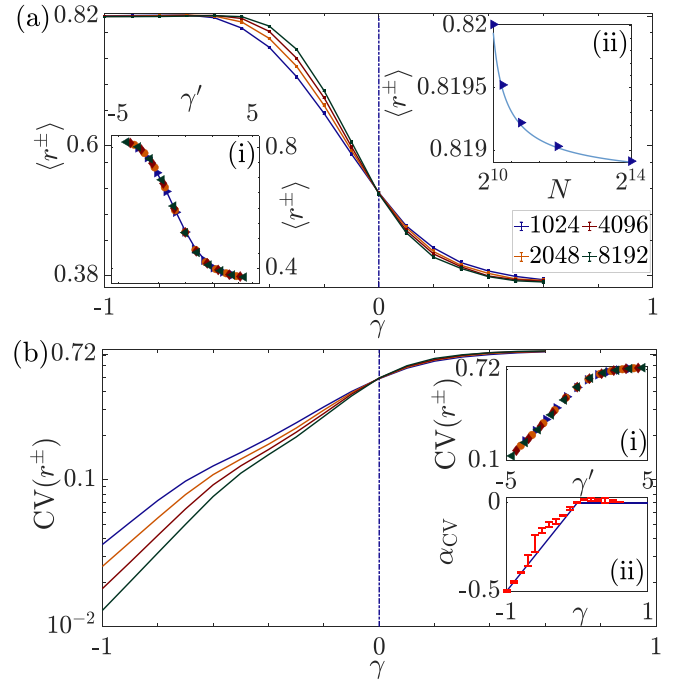


FIG. 6. Level-spacing ratio  $r^\pm$  at edge of the spectrum: (a) ensemble-averaged  $\langle r^\pm \rangle$ . Inset (i) shows the collapsed data assuming second-order phase transition. Inset (ii) shows  $\langle r^\pm \rangle$  for the mean Hamiltonian vs  $N$ , Eq. (9). Solid line denotes power-law fitting:  $\langle r^\pm \rangle = 0.1158N^{-0.6543} + 0.8187$ . (b) Coefficient of variation,  $CV(r) \equiv \sqrt{\langle r^2 \rangle - \langle r \rangle^2} / \langle r \rangle$ . Inset (i) shows collapsed data, whereas inset (ii) shows system-size scaling, i.e.,  $CV(r^\pm) \propto N^{\alpha_{CV}}$ .

polynomials for the large argument

$$\mathcal{H}_n(x)|_{|x| \rightarrow \infty} = (2x)^n \left( 1 - \frac{n(n-1)}{(2x)^2} + \mathcal{O}(x^{-4}) \right). \quad (13)$$

The second term in the above expansion can be neglected for  $x \gtrsim \frac{\sqrt{n(n-1)}}{2}$  or equivalently at  $n \lesssim 2x$ . Then the scaling of  $E$  with  $N$  in  $x$ , Eq. (10), implies that for  $|E| \gtrsim N^{-\frac{\gamma}{2}} \sqrt{\frac{n(n-1)}{2}}$ , or equivalently, for  $n \lesssim |E|N^{\frac{\gamma}{2}}$ ,  $\mathcal{H}_n(\lambda) \sim (|E|N^{\frac{\gamma}{2}})^n$  and, thus, the eigenstate with energy  $E$  decays with  $m = N - n$  as

$$\Psi_E(m) = \frac{(|E|N^{\frac{\gamma}{2}})^{N-m}}{\sqrt{(N-m)!}} \approx \mathcal{Z} \left( \frac{|E|}{N^{\frac{1-\gamma}{2}}} \sqrt{\frac{e}{1 - \frac{m}{N}}} \right)^{N-m}. \quad (14)$$

The largest root of the  $n$ th Hermite polynomial  $\mathcal{H}_n(x)$  is at  $x \approx \sqrt{2n}$ ; see Eq. (12) for  $N \rightarrow n$ . Then  $\mathcal{H}_n(x)$  oscillates as a function of  $n$  without causing any decay in the eigenstate (10) at  $n \gtrsim \frac{x^2}{2} = \frac{E^2}{3N^{-\gamma}}$ . On the other hand, there is a decay slower than that in Eq. (14) within the interval  $2x \lesssim n \lesssim \frac{x^2}{2}$ , where no zeros of  $H_n(x)$  are present. All these three intervals describe the spatial behavior of the eigenstates for  $\gamma < 0$ , see Fig. 4.

In the inset of Fig. 4(c), we show the finite-size fractal dimension  $D_2^{(N)} \equiv -\log_N I_2$  of  $\bar{H}$  as a function of  $1/\log N$ , indicating that  $D_2 \approx D_2^{(N)} - c/\log N$  where  $D_2 \approx 1/3$  is the

true fractal dimension of the ground state of  $\overline{H}$ . In Fig. 4(c) we show  $D_2$  as a function of  $\gamma$  for the  $\beta$  ensemble. We find that  $D_2 \approx 1/3$  for  $\gamma \leq 0$ , therefore matching with the prediction from  $\overline{H}$ . Therefore the ground state has a fractal dimension three times smaller than that of the bulk states in the entire parameter regime of the  $\beta$  ensemble.

## V. CONCLUSIONS

Motivated by the peculiarity of the ground-state physics in quantum chaotic many-body systems [13], we consider the ground and anti-ground states of the  $\beta$  ensemble in this work. We show that in the extended phase ( $\gamma < 1$ ), the ground state of the  $\beta$  ensemble exhibits nonergodic properties with the fractal dimension, being three times smaller than its bulk value. The localization centers of these spectral edge states are exponentially distributed close to those of the most delocalized states, while the widths of the density of localization centers scale nontrivially with the system size.

The main difference between the low-energy physics of the region  $\gamma < 0$  and nonergodic phase ( $0 < \gamma < 1$ ) is the correlations between the ground and the anti-ground states. In the nonergodic phase, these two edge states do not hybridize while the respective localization centers and the energies are uncorrelated. In contrast, the correlations become rigid for  $\gamma < 0$ : adjacent level repulsion is strong while the ground and anti-ground states have a perfect overlap.

In both the localized and the extended nonergodic phases, the spatial local mapping to the 1D Anderson model as suggested in [36] provide analytical understanding of the above results in the NEE phase. Using the standard weak-disorder limit for the spectral edge states, we found the ground-state fractal dimension to be one-third of its bulk value while the ground and anti-ground states remain uncorrelated. On the other hand, for  $\gamma < 0$  the physics is controlled by the mean Hamiltonian matrix, and we have explicitly computed the corresponding eigenstates and eigenvalues. Hence, we claim that similar to the quantum chaotic many-body models, the  $\beta$  ensemble shows a peculiar fractal structure of the ground-state eigenfunctions, even for a highly correlated energy spectrum ( $\gamma < 0$ ). It will be of particular interest to see how the nonergodicity of the ground state affects the finer structures of the bulk states, e.g., the possibility of a Hilbert space blockade [101–107]. Such a constraint can enforce weak ergodicity leading to nontrivial thermalization, similarly to other random-matrix models [59,72,108] and random graphs [109–113].

## ACKNOWLEDGMENTS

A.K.D. is supported by an INSPIRE Fellowship, DST, India, and by Fulbright-Nehru Grant No. 2879/FNDR/2023-2024. I.M.K. acknowledges the support by the European Research Council under the European Union's Seventh Framework Program Synergy ERC-2018-SyG HERO-810451.

## APPENDIX A: ENERGY-WINDOW SIZE OF SPECTRAL EDGE PHYSICS IN THE ERGODIC PHASE

In the parameter region  $\gamma \leq 0$ , the DOS of the  $\beta$  ensemble follows the semicircle law,  $\rho(E) = \frac{2}{\pi} \sqrt{1 - E^2}$ , upon scaling the energy spectrum as  $E \rightarrow E/2\sqrt{\langle E^2 \rangle}$ , where  $\langle E^2 \rangle \approx N^{1-\gamma}$  is the variance of the DOS [36]. In the interval  $[1 - \Delta, 1]$ , if only the edge states are present, then  $N \int_{1-\Delta}^1 dE \rho(E) = \mathcal{O}(1)$ . Note that [114]

$$\begin{aligned} \int_{1-\Delta}^1 dE \rho(E) &= \frac{1}{\pi} \left( 2 \sin^{-1} \sqrt{\frac{\Delta}{2}} + (\Delta - 1) \sqrt{\Delta(2 - \Delta)} \right) \\ &= \frac{4\sqrt{2}}{3\pi} \Delta^{\frac{3}{2}} + \mathcal{O}(\Delta^{\frac{5}{2}}) \\ &\Rightarrow N \times \Delta^{\frac{3}{2}} = \mathcal{O}(1) \\ &\Rightarrow \Delta = \mathcal{O}(N^{-\frac{2}{3}}). \end{aligned} \quad (\text{A1})$$

Then the actual width of the energy window containing the edge states is

$$\Delta_{\text{edge}} = \sqrt{\langle E^2 \rangle} \times \Delta = \mathcal{O}(N^{-\frac{3\gamma+1}{6}}). \quad (\text{A2})$$

## APPENDIX B: $r$ STATISTICS AT SPECTRAL EDGES IN THE ERGODIC PHASE

To quantify the short-range energy correlations at the edge of the spectrum, we look at the ratio of the level spacing between the edge state energies,  $r^\pm = \min\{\tilde{r}^\pm, \frac{1}{\tilde{r}^\pm}\}$ , where  $\tilde{r}^- = \frac{E_3 - E_2}{E_2 - E_1}$  and  $\tilde{r}^+ = \frac{E_N - E_{N-1}}{E_{N-1} - E_{N-2}}$  [99,100], assuming the eigenvalues are in the ascending order. In Fig. 6(a) we show ensemble-averaged  $r^\pm$  as a function of  $\gamma$  for various system sizes. Inset (i) shows that  $r^\pm$  undergoes a second-order transition at  $\gamma = 0$ . In inset (ii) we show the  $r^\pm$  for the Hamiltonian  $\overline{H}$  in Eq. (9) as a function of system size, which can be fitted using a power-law function. Thus  $\langle r^\pm \rangle \rightarrow 0.8187$  in the thermodynamic limit for  $\overline{H}$ , which is also the  $r^\pm$  observed for the  $\beta$  ensemble in the ergodic regime for  $N \gg 1$ . Note that in the bulk spectrum, the level-spacing ratio becomes unity in the thermodynamic limit owing to the full rigidity of the picket-fence structure of the energy spectrum [115].

In Fig. 6(b) we show the coefficient of variation of  $r^\pm$  as a function of  $\gamma$ . We observe that  $\text{CV}(r^\pm)$  also undergoes second-order transition at  $\gamma = 0$  [inset (i)]. For  $\gamma > 0$ ,  $\text{CV}(r^\pm)$  converges towards the Poisson limit,

$$\text{CV}_{\text{Poisson}} = \sqrt{\frac{3 - 2 \ln 4}{(\ln 4 - 1)^2}} - 1 \approx 0.723855. \quad (\text{B1})$$

Inset (ii) shows the system-size scaling of  $\text{CV}(r^\pm) \propto N^{\alpha_{\text{cv}}}$  where

$$\alpha_{\text{cv}} = \begin{cases} \frac{\gamma}{2}, & \gamma < 0 \\ 0, & \gamma \geq 0. \end{cases} \quad (\text{B2})$$

[1] J. M. Deutsch, Quantum statistical mechanics in a closed system, *Phys. Rev. A* **43**, 2046 (1991).

[2] M. Srednicki, Chaos and quantum thermalization, *Phys. Rev. E* **50**, 888 (1994).

- [3] M. Srednicki, Thermal fluctuations in quantized chaotic systems, *J. Phys. A: Math. Gen.* **29**, L75 (1996).
- [4] R. Marcos, D. Vanja, and O. Maxim, Thermalization and its mechanism for generic isolated quantum systems, *Nature (London)* **452**, 854 (2008).
- [5] A. Polkovnikov, K. Sengupta, A. Silva, and M. Vengalattore, Colloquium: Nonequilibrium dynamics of closed interacting quantum systems, *Rev. Mod. Phys.* **83**, 863 (2011).
- [6] J. Bardeen, L. N. Cooper, and J. R. Schrieffer, Theory of superconductivity, *Phys. Rev.* **108**, 1175 (1957).
- [7] R. B. Laughlin, Anomalous quantum Hall effect: An incompressible quantum fluid with fractionally charged excitations, *Phys. Rev. Lett.* **50**, 1395 (1983).
- [8] C. Monthus, Pure and random quantum Ising chain: Shannon and Rényi entropies of the ground state via real space renormalization, *J. Stat. Mech.: Theory Exp.* (2015) P04007.
- [9] D. J. Luitz, F. Alet, and N. Laflorencie, Universal behavior beyond multifractality in quantum many-body systems, *Phys. Rev. Lett.* **112**, 057203 (2014).
- [10] N. Moll, P. Barkoutsos, L. S. Bishop, J. M. Chow, A. Cross, D. J. Egger, S. Filipp, A. Fuhrer, J. M. Gambetta, M. Ganzhorn *et al.*, Quantum optimization using variational algorithms on near-term quantum devices, *Quantum Sci. Technol.* **3**, 030503 (2018).
- [11] A. K. Das, P. Pinney, D. A. Zarate-Herrada, S. Pilatowsky-Cameo, A. S. Matsoukas-Roubas, D. G. A. Cabral, C. Cianci, V. S. Batista, A. del Campo, E. J. Torres-Herrera, and L. F. Santos, Proposal for many-body quantum chaos detection, [arXiv:2401.01401](https://arxiv.org/abs/2401.01401).
- [12] J.-M. Stéphan, S. Furukawa, G. Misguich, and V. Pasquier, Shannon and entanglement entropies of one- and two-dimensional critical wave functions, *Phys. Rev. B* **80**, 184421 (2009).
- [13] Y. Y. Atas and E. Bogomolny, Multifractality of eigenfunctions in spin chains, *Phys. Rev. E* **86**, 021104 (2012).
- [14] Y. Y. Atas and E. Bogomolny, Calculation of multi-fractal dimensions in spin chains, *Philos. Trans. R. Soc. London, Ser. A*, **372**, 20120520 (2014).
- [15] G. Vidal, J. I. Latorre, E. Rico, and A. Kitaev, Entanglement in quantum critical phenomena, *Phys. Rev. Lett.* **90**, 227902 (2003).
- [16] J. Lindinger, A. Buchleitner, and A. Rodríguez, Many-body multifractality throughout bosonic superfluid and Mott insulator phases, *Phys. Rev. Lett.* **122**, 106603 (2019).
- [17] L. Amico, R. Fazio, A. Osterloh, and V. Vedral, Entanglement in many-body systems, *Rev. Mod. Phys.* **80**, 517 (2008).
- [18] A. Osterloh, L. Amico, G. Falci, and R. Fazio, Scaling of entanglement close to a quantum phase transition, *Nature (London)* **416**, 608 (2002).
- [19] T. J. Osborne and M. A. Nielsen, Entanglement in a simple quantum phase transition, *Phys. Rev. A* **66**, 032110 (2002).
- [20] L.-A. Wu, M. S. Sarandy, and D. A. Lidar, Quantum phase transitions and bipartite entanglement, *Phys. Rev. Lett.* **93**, 250404 (2004).
- [21] S. Sachdev, Quantum phase transitions, *Phys. World* **12**, 33 (1999).
- [22] W. Buijsman, T. L. M. Lezama, T. Leiser, and L. F. Santos, Ground-state energy distribution of disordered many-body quantum systems, *Phys. Rev. E* **106**, 054144 (2022).
- [23] V. Balasubramanian, J. M. Magan, and Q. Wu, A tale of two Hungarians: Tridiagonalizing random matrices, [arXiv:2208.08452](https://arxiv.org/abs/2208.08452).
- [24] D. E. Parker, X. Cao, A. Avdoshkin, T. Scaffidi, and E. Altman, A universal operator growth hypothesis, *Phys. Rev. X* **9**, 041017 (2019).
- [25] J. Ramírez, B. Rider, and B. Virág, Beta ensembles, stochastic airy spectrum, and a diffusion, *J. Am. Math. Soc.* **24**, 919 (2011).
- [26] J. T. Albrecht, C. P. Chan, and A. Edelman, Sturm sequences and random eigenvalue distributions, *Found. Comput. Math.* **9**, 461 (2009).
- [27] L. Dumaz and B. Virág, The right tail exponent of the Tracy–Widom  $\beta$  distribution, *Ann. Inst. H. Poincaré Probab. Statist., Probabilités et Statistiques* **49**, 915 (2013).
- [28] G. Borot, B. Eynard, S. N. Majumdar, and C. Nadal, Large deviations of the maximal eigenvalue of random matrices, *J. Stat. Mech.: Theory Exp.* (2011) P11024.
- [29] R. Allez and L. Dumaz, Tracy–Widom at high temperature, *J. Stat. Phys.* **156**, 1146 (2014).
- [30] A. Edelman, P.-O. Persson, and B. D. Sutton, Low-temperature random matrix theory at the soft edge, *J. Math. Phys.* **55**, 063302 (2014).
- [31] P. J. Forrester and A. K. Trinh, Optimal soft edge scaling variables for the Gaussian and Laguerre even  $\beta$  ensembles, *Nucl. Phys. B* **938**, 621 (2019).
- [32] K. Johansson, From Gumbel to Tracy–Widom, *Probab. Theory Relat. Fields* **138**, 75 (2007).
- [33] P. J. Forrester, Spectral density asymptotics for Gaussian and Laguerre  $\beta$ -ensembles in the exponentially small region, *J. Phys. A: Math. Theor.* **45**, 075206 (2012).
- [34] S. Kumar, Recursion for the smallest eigenvalue density of  $\beta$ -Wishart–Laguerre ensemble, *J. Stat. Phys.* **175**, 126 (2019).
- [35] F. Izrailev, S. Ruffo, and L. Tessieri, Classical representation of the one-dimensional Anderson model, *J. Phys. A: Math. Gen.* **31**, 5263 (1998).
- [36] A. K. Das, A. Ghosh, and I. M. Khaymovich, Absence of mobility edge in short-range uncorrelated disordered model: Coexistence of localized and extended states, *Phys. Rev. Lett.* **131**, 166401 (2023).
- [37] A. Gorsky, S. Nechaev, and A. Valov, On statistical models on super trees, *J. High Energy Phys.* **08** (2018) 123.
- [38] J. Breuer, P. J. Forrester, and U. Smilansky, Random discrete Schrödinger operators from random matrix theory, *J. Phys. A: Math. Theor.* **40**, F161 (2007).
- [39] F. J. Dyson, Statistical theory of the energy levels of complex systems. I, *J. Math. Phys.* **3**, 140 (1962).
- [40] P. Forrester, Beta ensembles, in *The Oxford Handbook of Random Matrix Theory* (Oxford University Press, Oxford, England, 2011).
- [41] I. Dumitriu and A. Edelman, Matrix models for beta ensembles, *J. Math. Phys.* **43**, 5830 (2002).
- [42] A. K. Das and A. Ghosh, Nonergodic extended states in the  $\beta$  ensemble, *Phys. Rev. E* **105**, 054121 (2022).
- [43] F. Nakano and K. D. Trinh, Gaussian beta ensembles at high temperature: eigenvalue fluctuations and bulk statistics, *J. Stat. Phys.* **173**, 295 (2018).
- [44] J. A. Cuesta and A. Sánchez, General non-existence theorem for phase transitions in one-dimensional systems with short

- range interactions, and physical examples of such transitions, *J. Stat. Phys.* **115**, 869 (2004).
- [45] M. Albert and P. Leboeuf, Localization by bichromatic potentials versus Anderson localization, *Phys. Rev. A* **81**, 013614 (2010).
- [46] V. E. Kravtsov, I. M. Khaymovich, E. Cuevas, and M. Amini, A random matrix model with localization and ergodic transitions, *New J. Phys.* **17**, 122002 (2015).
- [47] X. Deng, S. Ray, S. Sinha, G. V. Shlyapnikov, and L. Santos, One-dimensional quasicrystals with power-law hopping, *Phys. Rev. Lett.* **123**, 025301 (2019).
- [48] S. N. Evangelou and J.-L. Pichard, Critical quantum chaos and the one-dimensional Harper model, *Phys. Rev. Lett.* **84**, 1643 (2000).
- [49] S. Ray, A. Ghosh, and S. Sinha, Drive-induced delocalization in the Aubry-André model, *Phys. Rev. E* **97**, 010101(R) (2018).
- [50] E. J. Torres-Herrera and L. F. Santos, Extended nonergodic states in disordered many-body quantum systems, *Ann. Phys.* **529**, 1600284 (2017).
- [51] P. A. Nosov, I. M. Khaymovich, and V. E. Kravtsov, Correlation-induced localization, *Phys. Rev. B* **99**, 104203 (2019).
- [52] D.-Z. Wang, H. Zhu, J. Cui, J. Argüello-Luengo, M. Lewenstein, G.-F. Zhang, P. Sierant, and S.-J. Ran, Eigenstate thermalization and its breakdown in quantum spin chains with inhomogeneous interactions, *Phys. Rev. B* **109**, 045139 (2024).
- [53] E. van Nieuwenburg, Y. Baum, and G. Refael, From Bloch oscillations to many-body localization in clean interacting systems, *Proc. Natl. Acad. Sci. USA* **116**, 9269 (2019).
- [54] O. Bohigas, M. J. Giannoni, and C. Schmit, Characterization of chaotic quantum spectra and universality of level fluctuation laws, *Phys. Rev. Lett.* **52**, 1 (1984).
- [55] M. Mehta, *Random Matrices*, Pure and Applied Mathematics, (Elsevier Science, New York, 2004).
- [56] M. Berry and M. Tabor, Level clustering in the regular spectrum, *Proc. R. Soc. London, Ser. A* **356**, 375 (1977).
- [57] D. Facoetti, P. Vivo, and G. Biroli, From non-ergodic eigenvectors to local resolvent statistics and back: A random matrix perspective, *Europhys. Lett.* **115**, 47003 (2016).
- [58] K. Truong and A. Ossipov, Eigenvectors under a generic perturbation: Non-perturbative results from the random matrix approach, *Europhys. Lett.* **116**, 37002 (2016).
- [59] C. Monthus, Statistical properties of the Green function in finite size for Anderson localization models with multifractal eigenvectors, *J. Phys. A: Math. Theor.* **50**, 295101 (2017).
- [60] P. von Soosten and S. Warzel, Non-ergodic delocalization in the Rosenzweig-Porter model, *Lett. Math. Phys.* **109**, 905 (2019).
- [61] E. Bogomolny and M. Sieber, Eigenfunction distribution for the Rosenzweig-Porter model, *Phys. Rev. E* **98**, 032139 (2018).
- [62] D. Venturelli, L. F. Cugliandolo, G. Schehr, and M. Tarzia, Replica approach to the generalized Rosenzweig-Porter model, *SciPost Phys.* **14**, 110 (2023).
- [63] G. Biroli and M. Tarzia, Lévy-Rosenzweig-Porter random matrix ensemble, *Phys. Rev. B* **103**, 104205 (2021).
- [64] W. Buijsman and Y. B. Lev, Circular Rosenzweig-Porter random matrix ensemble, *SciPost Phys.* **12**, 082 (2022).
- [65] I. M. Khaymovich, V. E. Kravtsov, B. L. Altshuler, and L. B. Ioffe, Fragile extended phases in the log-normal Rosenzweig-Porter model, *Phys. Rev. Res.* **2**, 043346 (2020).
- [66] A. K. Das and A. Ghosh, Eigenvalue statistics for generalized symmetric and Hermitian matrices, *J. Phys. A: Math. Theor.* **52**, 395001 (2019).
- [67] A. K. Das and A. Ghosh, Chaos due to symmetry-breaking in deformed Poisson ensemble, *J. Stat. Mech.: Theory Exp.* (2022) 063101.
- [68] A. K. Das and A. Ghosh, Transport in deformed centrosymmetric networks, *Phys. Rev. E* **106**, 064112 (2022).
- [69] F. Evers and A. D. Mirlin, Fluctuations of the inverse participation ratio at the Anderson transition, *Phys. Rev. Lett.* **84**, 3690 (2000).
- [70] A. D. Mirlin and F. Evers, Multifractality and critical fluctuations at the Anderson transition, *Phys. Rev. B* **62**, 7920 (2000).
- [71] P. Cizeau and J. P. Bouchaud, Theory of Lévy matrices, *Phys. Rev. E* **50**, 1810 (1994).
- [72] I. M. Khaymovich and V. E. Kravtsov, Dynamical phases in a “multifractal” Rosenzweig-Porter model, *SciPost Phys.* **11**, 045 (2021).
- [73] W. Tang and I. M. Khaymovich, Non-ergodic delocalized phase with Poisson level statistics, *Quantum* **6**, 733 (2022).
- [74] S. Roy, S. Basu, and I. M. Khaymovich, Ergodicity-breaking phase diagram and fractal dimensions in long-range models with generically correlated disorder, [arXiv:2307.03085](https://arxiv.org/abs/2307.03085).
- [75] A. De Luca, B. L. Altshuler, V. E. Kravtsov, and A. Scardicchio, Anderson localization on the Bethe lattice: Non-ergodicity of extended states, *Phys. Rev. Lett.* **113**, 046806 (2014).
- [76] V. Kravtsov, B. Altshuler, and L. Ioffe, Non-ergodic delocalized phase in Anderson model on Bethe lattice and regular graph, *Ann. Phys.* **389**, 148 (2018).
- [77] M. Pino, V. E. Kravtsov, B. L. Altshuler, and L. B. Ioffe, Multifractal metal in a disordered Josephson junctions array, *Phys. Rev. B* **96**, 214205 (2017).
- [78] B. L. Altshuler and V. E. Kravtsov, Random Cantor sets and mini-bands in local spectrum of quantum systems, *Ann. Phys.* **452**, 169300 (2023).
- [79] C. R. Laumann, A. Pal, and A. Scardicchio, Many-body mobility edge in a mean-field quantum spin glass, *Phys. Rev. Lett.* **113**, 200405 (2014).
- [80] A. Kutlin and I. Khaymovich, Emergent fractal phase in energy stratified random models, *SciPost Phys.* **11**, 101 (2021).
- [81] N. Macé, F. Alet, and N. Laflorencie, Multifractal scalings across the many-body localization transition, *Phys. Rev. Lett.* **123**, 180601 (2019).
- [82] D. J. Luitz, N. Laflorencie, and F. Alet, Many-body localization edge in the random-field Heisenberg chain, *Phys. Rev. B* **91**, 081103(R) (2015).
- [83] D. J. Luitz, I. Khaymovich, and Y. Bar Lev, Multifractality and its role in anomalous transport in the disordered XXZ spin-chain, *SciPost Phys. Core* **2**, 006 (2020).
- [84] Y. Wang, L. Zhang, W. Sun, T.-F. J. Poon, and X.-J. Liu, Quantum phase with coexisting localized, extended, and critical zones, *Phys. Rev. B* **106**, L140203 (2022).
- [85] N. Roy, J. Sutradhar, and S. Banerjee, Diagnostics of nonergodic extended states and many body localization proximity effect through real-space and Fock-space excitations, *Phys. Rev. B* **107**, 115155 (2023).

- [86] V. Motamarri, A. S. Gorsky, and I. Khaymovich, Localization and fractality in disordered Russian doll model, *SciPost Phys.* **13**, 117 (2022).
- [87] X. Cai, L.-J. Lang, S. Chen, and Y. Wang, Topological superconductor to Anderson localization transition in one-dimensional incommensurate lattices, *Phys. Rev. Lett.* **110**, 176403 (2013).
- [88] W. DeGottardi, D. Sen, and S. Vishveshwara, Majorana fermions in superconducting 1D systems having periodic, quasiperiodic, and disordered potentials, *Phys. Rev. Lett.* **110**, 146404 (2013).
- [89] J. Wang, X.-J. Liu, G. Xianlong, and H. Hu, Phase diagram of a non-Abelian Aubry-André-Harper model with  $p$ -wave superfluidity, *Phys. Rev. B* **93**, 104504 (2016).
- [90] J. Fraxanet, U. Bhattacharya, T. Grass, D. Rakshit, M. Lewenstein, and A. Dauphin, Topological properties of the long-range Kitaev chain with Aubry-André-Harper modulation, *Phys. Rev. Res.* **3**, 013148 (2021).
- [91] J. Fraxanet, U. Bhattacharya, T. Grass, M. Lewenstein, and A. Dauphin, Localization and multifractal properties of the long-range Kitaev chain in the presence of an Aubry-André-Harper modulation, *Phys. Rev. B* **106**, 024204 (2022).
- [92] J. Gao, I. M. Khaymovich, X.-W. Wang, Z.-S. Xu, A. Iovan, G. Krishna, A. V. Balatsky, V. Zwiller, and A. W. Elshaari, Experimental probe of multi-mobility edges in quasiperiodic mosaic lattices, [arXiv:2306.10829](https://arxiv.org/abs/2306.10829).
- [93] Z.-S. Xu, J. Gao, A. Iovan, I. M. Khaymovich, V. Zwiller, and A. W. Elshaari, Observation of reentrant metal-insulator transition in a random-dimer disordered SSH lattice, [arXiv:2307.05207](https://arxiv.org/abs/2307.05207).
- [94] X. Zhang, W. Zhang, J. Che, and B. Dietz, Experimental test of the Rosenzweig-Porter model for the transition from Poisson to Gaussian unitary ensemble statistics, *Phys. Rev. E* **108**, 044211 (2023).
- [95] A. Relaño, L. Muñoz, J. Retamosa, E. Faleiro, and R. A. Molina, Power-spectrum characterization of the continuous Gaussian ensemble, *Phys. Rev. E* **77**, 031103 (2008).
- [96] N. Mott, Electrons in disordered structures, *Adv. Phys.* **16**, 49 (1967).
- [97] F. M. Izrailev, T. Kottos, and G. P. Tsironis, Hamiltonian map approach to resonant states in paired correlated binary alloys, *Phys. Rev. B* **52**, 3274 (1995).
- [98] G. Szegő, *Orthogonal Polynomials*, No. Bd. 23 in American Mathematical Society Colloquium Publications (American Mathematical Society, Providence, RI, 1959).
- [99] V. Oganesyan and D. A. Huse, Localization of interacting fermions at high temperature, *Phys. Rev. B* **75**, 155111 (2007).
- [100] Y. Y. Atas, E. Bogomolny, O. Giraud, and G. Roux, Distribution of the ratio of consecutive level spacings in random matrix ensembles, *Phys. Rev. Lett.* **110**, 084101 (2013).
- [101] M. Haque, P. A. McClarty, and I. M. Khaymovich, Entanglement of midspectrum eigenstates of chaotic many-body systems: Reasons for deviation from random ensembles, *Phys. Rev. E* **105**, 014109 (2022).
- [102] Y. Huang, Universal eigenstate entanglement of chaotic local Hamiltonians, *Nucl. Phys. B* **938**, 594 (2019).
- [103] Y. Huang, Universal entanglement of mid-spectrum eigenstates of chaotic local Hamiltonians, *Nucl. Phys. B* **966**, 115373 (2021).
- [104] L. Pausch, E. G. Carnio, A. Rodríguez, and A. Buchleitner, Chaos and ergodicity across the energy spectrum of interacting bosons, *Phys. Rev. Lett.* **126**, 150601 (2021).
- [105] L. Pausch, E. G. Carnio, A. Buchleitner, and A. Rodríguez, Chaos in the Bose-Hubbard model and random two-body Hamiltonians, *New J. Phys.* **23**, 123036 (2021).
- [106] M. Kliczkowski, R. Świątek, L. Vidmar, and M. Rigol, Average entanglement entropy of midspectrum eigenstates of quantum-chaotic interacting Hamiltonians, *Phys. Rev. E* **107**, 064119 (2023).
- [107] A. Sarkar and S. Kumar, Entanglement spectrum statistics of a time reversal invariant spin chain system: Insights from random matrix theory, *Eur. Phys. J. B* **96**, 120 (2023).
- [108] A. K. Das and A. Ghosh, Dynamical signatures of Chaos to integrability crossover in  $2 \times 2$  generalized random matrix ensembles, *J. Phys. A: Math. Theor.* **56**, 495003 (2023).
- [109] G. Biroli and M. Tarzia, Delocalized glassy dynamics and many-body localization, *Phys. Rev. B* **96**, 201114(R) (2017).
- [110] S. Bera, G. De Tomasi, I. M. Khaymovich, and A. Scardicchio, Return probability for the Anderson model on the random regular graph, *Phys. Rev. B* **98**, 134205 (2018).
- [111] G. De Tomasi, S. Bera, A. Scardicchio, and I. M. Khaymovich, Subdiffusion in the Anderson model on the random regular graph, *Phys. Rev. B* **101**, 100201(R) (2020).
- [112] G. Biroli and M. Tarzia, Anomalous dynamics on the ergodic side of the many-body localization transition and the glassy phase of directed polymers in random media, *Phys. Rev. B* **102**, 064211 (2020).
- [113] L. Colmenarez, D. J. Luitz, I. M. Khaymovich, and G. De Tomasi, Subdiffusive Thouless time scaling in the Anderson model on random regular graphs, *Phys. Rev. B* **105**, 174207 (2022).
- [114] S. N. Majumdar and G. Schehr, Top eigenvalue of a random matrix: Large deviations and third order phase transition, *J. Stat. Mech.: Theory Exp.* (2014) P01012.
- [115] A. Pandey and R. Ramaswamy, Level spacings for harmonic-oscillator systems, *Phys. Rev. A* **43**, 4237 (1991).